Supplementary information for "Ultrafast dynamics in polycyclic aromatic hydrocarbons: the key case of conical intersections in higher excited states and their role in the photophysics of phenanthrene monomer"

M. Nazari [a], C. D. Bösch [b], A. Rondi [a], A. Francés Monerris [c], M. Marazzi [c,d,e], E. Lognon [c], M. Gazzetto [a], S. M. Langenegger [b], R. Häner [b], T. Feurer [a], A. Monari*[c], and A. Cannizzo *[c]

[a] Institute of Applied Physics, University of Bern, Switzerland

[b] Department of Chemistry and Biochemistry, University of Bern, Switzerland

[c] Université de Lorraine & CNRS, LPCT UMR 7019, Nancy, France

[d] Department of Analytical Chemistry, Physical Chemistry and Chemical Engineering, University of Alcalà, Spain

[e] Chemical Research Institute "Andrés M. del Río" (IQAR), University of Alcalà, Spain

* andrea.cannizzo@iap.unibe.ch, antonio.monari@univ-lorraine.fr

This file includes

A: Calculation of TA signal in single-shot detection

B: Tentative photocycle derived from the analysis of the experimental data only

C: TD-DFT calculations

D: Details on multiconfigurational calculations and calibration of the molecular models and the TD-DFT method

E: Non-adiabatic molecular dynamics simulations

F: xyz coordinates of the moist relevant stationary points as obtained by molecular modeling

A: Calculation of TA signal in single-shot detection

The TA signal in single-shot detection scheme (in the following $TA_i(\lambda,t)$) is calculated by recording and subtracting two sequential shots, unpumped (I_U) and pumped probe spectra (I_P), which are obtained by the use of a chopper in the pump beamline with the circular frequency of 2.5 KHz, for each delay point. A photo-diode after the chopper was used to monitor shot-to-shot pulse intensity in order to sort 'pumped' and 'unpumped' measurements and to compensate for fluctuations and drifts with respect to the intensity of the pump pulse in the first shot. Spectral- and amplitude fluctuations of the continuum spectrum were corrected shot-to-shot by dividing the probe spectrum by the reference one. Applying all these corrections, the single-shot TA signals ($TA_i(\lambda,t)$) for each time-delay was calculated as:

$$TA_i(\lambda,t) = \frac{-2}{ln(10)}\left(\frac{p_0}{p_i}\right)\left(\frac{\dfrac{I_{S,P,i}(\lambda,t)}{I_{r,P,i}(\lambda,t)} - \dfrac{I_{S,U,i}(\lambda,t)}{I_{r,U,i}(\lambda,t)}}{\dfrac{I_{S,P,i}(\lambda,t)}{I_{r,P,i}(\lambda,t)} + \dfrac{I_{U,i}(\lambda,t)}{I_{r,U,i}(\lambda,t)}}\right) \qquad \text{eq. S1}$$

Where each continuum spectrum $I(t,\lambda)$ recorded by the camera is indexed by i for each pair of consecutive pumped and unpumped probe spectra. The indices S and r refer to probe and reference pulses, respectively and the indices P and U refer to pumped and unpumped signals, respectively. The pump fluctuation correction is accounted for by the fraction p_o/p_i where p_o and p_i are the pump intensity recorded at the beginning of a scan and at delay i. To decrease the statistical noise and achieve a better signal-to-noise ratio we average the signal over several shots (5000 shots). The averaged signal over *n* numuber of shots was then calculated accordingly to the following equation:

$$TA(t,\lambda) = \frac{1}{n}\sum_{i=1}^{n} TA_i(t,\lambda) \qquad \text{eq. S2}$$

B: Tentative photocycle derived from the analysis of the experimental data only
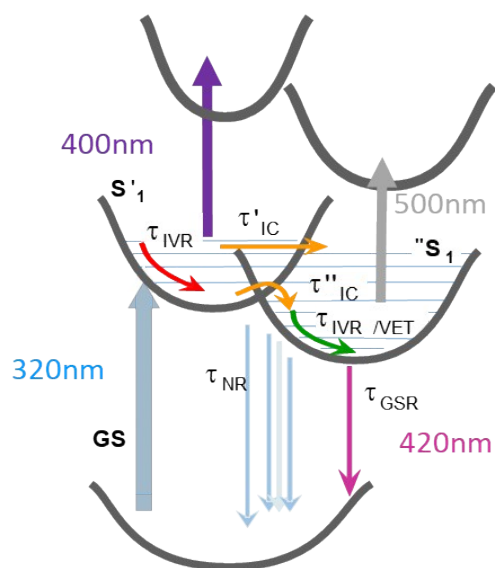

Figure S1: a tentative photocycle which had been derived only from the analysis of the experimental data and before having the information from TD-DFT calculations (see Figure 2 and related discussion). Notation: IVR, internal vibrational redistribution; IC, internal conversion; VET, vibrational energy transfer (cooling); NR, non-radiative; GSR, ground state recovery. According to the data analysis reported in the main text, we can make the following correspondences: $\tau_{IVR} \sim \tau_1$, $\tau'_{IC} \sim \tau_2$, $\tau''_{IC} \sim \tau_3$, $\tau_{IVR/VET} \sim \tau_4$, $\tau_{GSB} \sim \tau_6$ (τ_5, the rotational diffusion term is not shown).
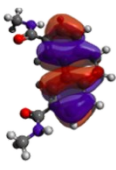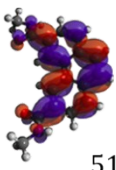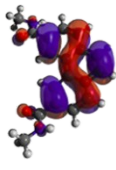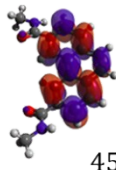
C: TD-DFT calculations

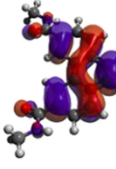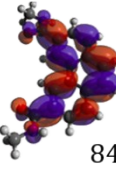|	Occupied	Virtual
S_A		51%
		45%
S_B		84%

Figure S2: Natural Transition Orbitals (NTO) [1-3] for the first two low lying excited states at the FC geometry. The corresponding weights in the expansion are reported too. For the convenience of the reader, we remind that NTOs, obtained via singular value decomposition of the transition density matrix, condense the relevant information on the electronic density reorganization via a transition between only one couple of orbitals: the occupied (hole) indicating the electron withdrawing, and the virtual (particle) indicating electron accumulation.
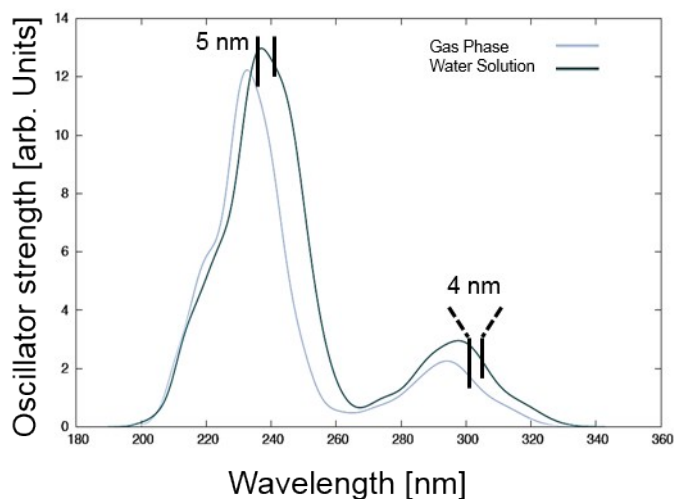

Figure S3: Calculated absorption spectra of phenanthrene monomers in vacuum and in water, the latter treated as a polarizable continuum model. A Wigner convolution was used to include vibrational broadening. The effects of solvent (water) induces only a very small blue shift of 4-5 nm.

D: Details on multiconfigurational calculations and calibration of the molecular models and the TD-DFT method

To validate the TD-DFT results, multiconfigurational calculations using the complete-active-space self-consistent field (CASSCF) and the complete-active-space second-order perturbation theory (CASPT2) methods were performed on top of the ground-state geometry of the phenanthrene monomer optimized at the DFT/ωB97XD level. The carboxamide substituents (see Figure 1 of the main text) were replaced by hydrogens in order to reduce the computational overload. The CASSCF wave functions were built by distributing 12 electrons into the 12 most relevant π-like molecular orbitals (MOs), hereafter CASSCF(12,12). The MOs are sketched in Figure S4. Even though the valence space of phenanthrene comprises 14 electrons, the CASSCF(12,12) space is expected to provide accurate energies, as documented in previous studies [4]. Eight states have been computed in the state-average (SA)-CASSCF procedure, and the atomic natural orbital (ANO) S-type basis set with the C,N[3s2p1d]/H[2s1p] contraction scheme (hereafter, ANO-S-VDZP) have been used throughout. No symmetry constraints were imposed in the computations.

The dynamic electronic correlation was computed by means of the CASPT2 method using the SA-CASSCF wave functions as reference. All core electrons were kept frozen during the perturbation step. The original CASPT2 zeroth-order Hamiltonian (IPEA = 0.0 a.u) was used throughout, and an imaginary level shift of 0.2 a.u was used to minimize the presence of weakly interacting intruder states. All multiconfigurational calculations were performed with the MOLCAS 8 software package [5].
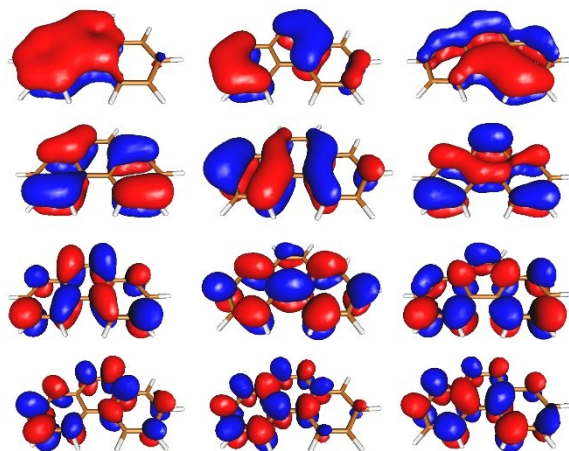

Figure S4: Natural CASSCF orbitals of phenanthrene included in the CASSCF(12,12) active space.

For calibration purposes, we have compared the excited-state properties of the systems **I** and **II**, displayed in Figure S5), computed at different levels of theory. The system **I** corresponds to phenanthrene and has been used for the multiconfigurational calculations. Moreover, the excitation properties of this system have been profusely documented in the literature. On the other hand, compound **II** is the monomer used in the experiments and in the static calculations reported in this work. Note that this nomenclature is only used in this subsection.

.
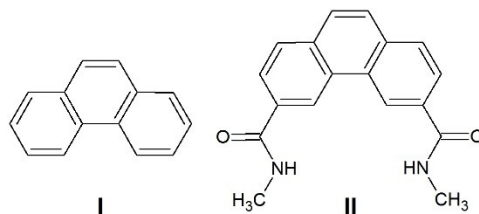
Figure S5: Structures of the model systems.

Table S1 compiles the present TD-DFT and CASPT2 vertical absorption energies obtained in the gas phase for phenanthrene **I**, in conjunction with previous theoretical determinations and experimental measurements taken from the literature. Our CASPT2 results are in good agreement (~0.2 eV of difference) with previous CASPT2 determinations reported by González-Luque *et al* [4]. The small discrepancies can be ascribed to the use of symmetry restrictions, a different basis set

4

contraction scheme, and to the larger imaginary level shift (0.3 au) set for the CASPT2 method. Overall, excellent agreement is found between the CASPT2 results and the experimental determinations also compiled by González-Luque *et al* (see Table S1). Wang and Wu [6] reported B3LYP determinations using the Tamm-Dancoff approximation which is also showing good agreement with the experimental recordings. The ωB97XD excitation energies lie above our CASPT2 determinations, however, the global description of the two lowest-lying excited states is satisfactory. The relative order of the energies and their associated oscillator strengths are coherent between both methodologies, in particular, the two states are separated by approximately the same amount of energy (~0.3 – 0.5 eV), and the oscillator strengths are very similar. Altogether, the present results validate the ωB97XD functional, which includes important dispersion corrections to represent van der Waals interactions, to study the excited sate PESs and dynamics of the phenanthrene systems considered in the present work at an affordable computational cost.

Table S1: Vertical excitation energies (in eV) and oscillator strengths (within parenthesis) for phenanthrene I in the gas phase. Present and previous TD-DFT and CASPT2 determinations and experimental measurements (also in eV) are shown. [a] from [6].

State	B3LYP[a]	B3LYP/TDA[b]	ωB97XD[c]	CASPT2/ ANO-321/2[d]	CASPT2/AN O-S-VDZP[e]	Exp[f]
$S_1 L_A$	3.23	3.79	4.26 (0.001)	3.42 (0.000)	3.64 (0.000)	3.51 – 3.68
$S_2 L_B$	3.50	4.35	4.54 (0.102)	4.37 (0.038)	4.14 (0.125)	4.09 – 4.36

[b] Tam-Dancoff Approximation (TDA), from [6].

[c] 6-31+G(d) basis set, present work.

[d] C_{2v} symmetry and the ANO basis set with the C,N[3s2p1d]/H[2s] contraction scheme. From [4]

[e] Present work.

[f] The ranges of experimental measurements are taken from Table 2 of [4]. The reader is referred to this article to find the specific experimental references.

The influence of the substituents on the excitation properties of the phenanthrene derivatives displayed in Figure S5 can be assessed by comparing the results summarized in Tables S1 and S2. The absence of the carboxamide links slightly increases the excitation energies of **I** by 0.10-0.15 eV, due to the small inductive effect of the hydrogen atoms. On the other hand, and as commented in Figure S3, the inclusion of the solvent effects by means of the PCM method only has a slight effect in the optically active transition, yielding a shift of a few nm.

Table S2: Vertical excitation energies (in eV) and oscillator strengths (within parenthesis) for phenanthrene derivatives II obtained with the 6-31+G(d) basis set. Present experimental measurements (also in eV) are shown.

State	ωB97XD[a]	ωB97XD/PCM[a]	Exp[a]
$S_1 L_A$	4.14 (0.006)	4.14 (0.010)	~4
$S_2 L_B$	4.31 (0.299)	4.25 (0.443)	

[a] Present work.

E: Non-adiabatic molecular dynamics simulations

The non-adiabatic molecular dynamics (NAMD) simulations have been run making use of the SHARC/ADF interface, in which the wave functions, energies and electronic gradients are computed with the ADF modelling suite, whereas the SHARC code computes the diabatic states and the hop probabilities between them, propagating the excited-state trajectory.

Since the TD-DFT excited-state gradients for the ωB97XD functional are not available in the ADF 2018 release, a different hybrid functional has been used, in particular the BHandHLYP functional. In addition, and with the aim to reduce the large computational overload of the study, a smaller double-zeta basis set (DZ) has been used for all the simulations. Benchmark calculations on the most relevant points of the PES of the phenanthrene derivative **II**, *i.e.* the ground state equilibrium geometry and the S_A and S_B optimized geometries, are displayed in Figure S6. Note that the same structures, optimized at the ωB97XD/6-31G* level of theory, have been used in the benchmark. The three studied levels of theory, namely the ωB97XD/6-31+G(d), ωB97XD/6-31G* and the BHandHLYP/DZ methods, provide coherent descriptions of the excited states of the system. Relatively small energy shifts (< 0.2 eV) are caused by the use of smaller basis sets, however, all the points

are equally affected. Thus, since shifting the PES does not affect the dynamical properties of the system, the present results validate the use of the BHandHLYP/DZ method as implemented in ADF2018 to perform NAMD simulations.
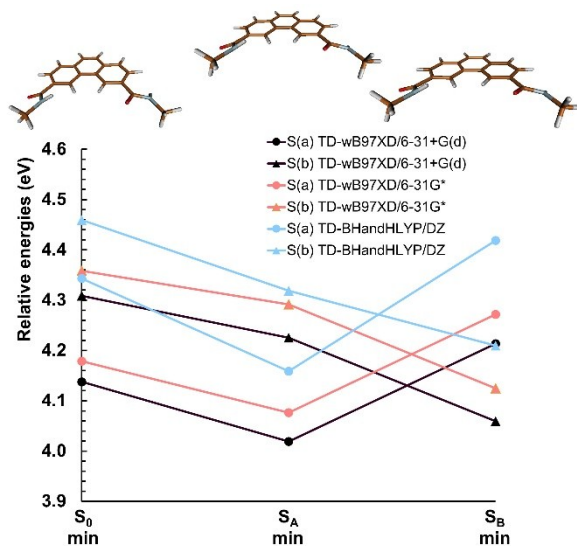

Figure S6: Benchmark of the TD-ωB97XD/6-31+G(d) and TD-ωB97XD/6-31G* methods (GAUSSIAN 09) and the TD-BH and HLYP/DZ level of theory (ADF2018).

The initial conditions (atomic coordinates and velocities) were obtained stochastically following the vibrational modes at the ground state equilibrium geometry by means of a Wigner sampling. The dynamics were run on diagonal PES computed using the surface-hopping including arbitrary couplings (SHARC) algorithm, resulting from the diagonalization of the Hamiltonian containing non-adiabatic couplings [7] [8]. The integration of the nuclear motion has been done by means of the Velocity-Verlet algorithm with a total simulation time of 1 ps and using a time step of 0.5 fs. Decoherence correction was included using the energy-based method of Granucci, Persico and Zoccante with the suggested parameter of C = 0.1 a.u [9].

F: xyz coordinates of the most important stationary points as obtained from molecular modeling

Franck-Condon region

C	-5.676798	2.477647	0.665533
C	-4.258388	2.675203	0.593291
C	-3.409778	1.589045	0.222855
C	-4.006561	0.292122	-0.073373
C	-5.422420	0.145246	0.009636
C	-6.232656	1.267561	0.385268
H	-7.309559	1.129178	0.441183
H	-6.302437	3.320043	0.950067
C	-3.683689	3.931664	0.894682
C	-2.021243	1.823737	0.165994
C	-3.241477	-0.836442	-0.441900
C	-6.009453	-1.107379	-0.288889
C	-1.471250	3.066899	0.444627
C	-2.320558	4.131085	0.823473
H	-1.325913	1.034493	-0.093662
H	-4.338399	4.745227	1.197492

6

```
C     0.024579    3.187627    0.338344
H    -1.907708    5.097307    1.099893
C    -3.832273   -2.063033   -0.715680
C    -5.237248   -2.188760   -0.651242
H    -5.679924   -3.147974   -0.896697
H    -7.091054   -1.203020   -0.230729
H    -2.167594   -0.731678   -0.549474
C    -3.051784   -3.284362   -1.121515
O     0.755816    2.200445    0.369671
N     0.519348    4.459006    0.212556
H    -0.121663    5.196523   -0.040837
C     1.939120    4.697824    0.015661
H     2.491968    3.924079    0.549581
H     2.205422    5.680434    0.416084
H     2.225135    4.654297   -1.043986
O    -3.578005   -4.198141   -1.751753
N    -1.732326   -3.307895   -0.756359
H    -1.417396   -2.649763   -0.058730
C    -0.888800   -4.456415   -1.039264
H    -1.256686   -4.931353   -1.949467
H    -0.913491   -5.198416   -0.229767
H     0.144064   -4.127919   -1.188559
```

*S*_{*A*} *minimum*

```
C    -5.681210    2.490077    0.673909
C    -4.288716    2.695974    0.585278
C    -3.419588    1.580486    0.209276
C    -4.000598    0.307708   -0.070466
C    -5.449616    0.143114    0.042745
C    -6.245552    1.248799    0.412455
H    -7.320899    1.114846    0.490933
H    -6.317671    3.324248    0.957224
C    -3.702432    3.944949    0.863240
C    -2.027776    1.822137    0.151559
C    -3.234760   -0.822754   -0.453565
C    -6.011740   -1.119308   -0.229330
C    -1.474151    3.074035    0.418085
C    -2.326499    4.142296    0.787502
H    -1.329178    1.032226   -0.097536
H    -4.346866    4.768850    1.158943
C     0.010840    3.192781    0.325289
H    -1.918849    5.110482    1.062427
C    -3.820329   -2.063770   -0.697007
C    -5.224552   -2.202982   -0.597842
H    -5.666872   -3.167990   -0.820209
H    -7.088680   -1.239963   -0.147470
H    -2.167090   -0.706124   -0.600449
C    -3.036699   -3.269123   -1.106016
O     0.741855    2.206285    0.370148
N     0.520389    4.452679    0.201210
H    -0.096320    5.199125   -0.079455
C     1.948153    4.653723    0.047183
H     2.477105    4.155756    0.862873
H     2.156874    5.724994    0.086026
```

H	2.317281	4.242510	-0.899567
O	-3.560482	-4.191865	-1.723596
N	-1.715261	-3.287600	-0.771790
H	-1.378589	-2.642681	-0.073788
C	-0.891982	-4.435873	-1.097969
H	-0.977602	-4.656580	-2.164252
H	-1.201027	-5.326908	-0.539270
H	0.148005	-4.200420	-0.862719

S_B minimum

C	-5.655627	2.493174	0.649510
C	-4.285284	2.698077	0.547989
C	-3.409027	1.598904	0.204920
C	-4.008908	0.278857	-0.063568
C	-5.441467	0.124141	0.070016
C	-6.230728	1.214138	0.419622
H	-7.305972	1.089015	0.511262
H	-6.303203	3.323681	0.918403
C	-3.696819	3.981159	0.803338
C	-2.048924	1.830199	0.159428
C	-3.260741	-0.821658	-0.448864
C	-6.017120	-1.165963	-0.188416
C	-1.481719	3.106749	0.400420
C	-2.336905	4.176998	0.732476
H	-1.342266	1.037684	-0.059924
H	-4.352897	4.805099	1.072667
C	-0.004500	3.207925	0.325885
H	-1.935274	5.156808	0.974990
C	-3.844512	-2.087294	-0.681348
C	-5.240998	-2.234504	-0.558502
H	-5.678449	-3.206218	-0.761739
H	-7.092902	-1.280464	-0.084069
H	-2.195500	-0.700892	-0.613893
C	-3.056379	-3.285969	-1.079954
O	0.712403	2.205739	0.354546
N	0.536134	4.462520	0.243797
H	-0.054470	5.225761	-0.046710
C	1.969603	4.629634	0.107253
H	2.478325	4.106500	0.920176
H	2.204166	5.694886	0.165311
H	2.340203	4.224098	-0.841962
O	-3.587645	-4.254471	-1.620070
N	-1.713236	-3.256502	-0.831329
H	-1.347498	-2.573886	-0.185796
C	-0.889345	-4.407258	-1.144970
H	-1.005909	-4.666407	-2.199893
H	-1.172635	-5.281539	-0.546971
H	0.154944	-4.154581	-0.950022

REFERENCES

1   R. L. Martin, *J. Chem. Phys.*, 2003, **118**, 4775–4777.

2   T. Etienne, X. Assfeld and A. Monari, *J. Chem. Theory Comput.*, 2014, **10**, 3896–3905.

3   T. Etienne, X. Assfeld and A. Monari, *J. Chem. Theory Comput.*, 2014, **10**, 3906–3914.

4   R. Gonzalez-Luque, L. Serrano-Andres, M. Mercha and M. P. Fülscher, *Theor. Chem. Acc.*, 2003, **110**, 224–232.

5   F. Aquilante, J. Autschbach, R. K. Carlson, L. F. Chibotaru, M. G. Delcey, L. De Vico, I. Fdez. Galván, N. Ferré, L. M. Frutos, L. Gagliardi, M. Garavelli, A. Giussani, C. E. Hoyer, G. Li Manni, H. Lischka, D. Ma, P. Å. Malmqvist, T. Müller, A. Nenov, M. Olivucci, T. B. Pedersen, D. Peng, F. Plasser, B. Pritchard, M. Reiher, I. Rivalta, I. Schapiro, J. Segarra-Martí, M. Stenrup, D. G. Truhlar, L. Ungur, A. Valentini, S. Vancoillie, V. Veryazov, V. P. Vysotskiy, O. Weingart, F. Zapata and R. Lindh, *J. Comput. Chem.*, 2016, **37**, 506–541.

6   T. D. Approximation, Y. Wang and G. Wu, 2008, **108**, 430–439.

7   S. Mai, P. Marquetand, M. Richter, J. González-Vázquez and L. González, *ChemPhysChem*, 2013, **14**, 2920–2931.

8   S. Mai, P. Marquetand and L. Gonz, *Int. J. Quantum Chem.*, 2015, **115**, 1215–1231.

9   G. Granucci, M. Persico, A. Zoccante, G. Granucci, M. Persico and A. Zoccante, *J. Chem. Phys.*, 2010, **133**, 134111–9.